

ARTICLE OPEN

High field charge order across the phase diagram of $\text{YBa}_2\text{Cu}_3\text{O}_y$ Francis Laliberté¹, Mehdi Frachet¹, Siham Benhabib¹, Benjamin Borgnic¹, Toshinao Loew², Juan Porras², Mathieu Le Tacon^{2,3}, Bernhard Keimer², Steffen Wiedmann⁴, Cyril Proust¹ and David LeBoeuf¹

In hole-doped cuprates there is now compelling evidence that inside the pseudogap phase, charge order breaks translational symmetry. In $\text{YBa}_2\text{Cu}_3\text{O}_y$ charge order emerges in two steps: a 2D order found at zero field and at high temperature inside the pseudogap phase, and a 3D order that is superimposed below the superconducting transition T_c when superconductivity is weakened by a magnetic field. Several issues still need to be addressed such as the effect of disorder, the relationship between those charge orders and their respective impact on the Fermi surface. Here, we report high magnetic field sound velocity measurements of the 3D charge order in underdoped $\text{YBa}_2\text{Cu}_3\text{O}_y$ in a large doping range. We found that the 3D charge order exists over the same doping range as its 2D counterpart, indicating an intimate connection between the two distinct orders. Moreover, our data suggest that 3D charge order has only a limited impact on low-lying electronic states of $\text{YBa}_2\text{Cu}_3\text{O}_y$.

npj Quantum Materials (2018)3:11 ; doi:10.1038/s41535-018-0084-5

INTRODUCTION

While both theoretical and experimental analysis have long suggested that charge order might play a significant role in the pseudogap phase of the cuprates, the more recent discovery of charge order in the putatively “cleanest” cuprate $\text{YBa}_2\text{Cu}_3\text{O}_y$ (YBCO) has triggered a surge of experimental^{1–5} and theoretical^{6–11} works. The relation between charge order and pseudogap is not yet settled but some models predict that they are intertwined.^{8–10} In some scenarios the pseudogap phase corresponds to a nematic phase precursor to charge ordering at lower temperature^{6,7} or to a fluctuating charge order.^{12,13} While superconductivity appears to compete with charge order experimentally, a class of theory suggests it could be collaborating.¹⁴ Two distinct charge orders have been detected in YBCO. First a two-dimensional (2D) short-range (but static) bidirectional charge density wave (CDW) appears at high temperature between T_c and the pseudogap temperature T^* . Comprehensive X-ray measurements^{15,16} in YBCO have shown that the 2D CDW is incommensurate and occurs in the doping range $p \approx 0.08$ to $p \approx 0.16$. The propagation vectors along a and b directions are $Q_a = (\delta_a, 0, 0.5)$ and $Q_b = (0, \delta_b, 0.5)$ where $\delta_{a,b} \approx 0.3–0.34$ with in-plane correlation lengths that are at most 20 unit cells and weak anti-phase correlation between neighboring bilayers. The short-range CDW has also been detected through a broadening of the NMR lines.¹⁷ The second CDW, originally detected using high field NMR,² appears below T_c and above a threshold field.^{2,18} Recent X-Ray measurements in high field have shown that it is a three-dimensional (3D) ordered state with in-plane CDW modulations along the b direction only—though at the same δ_b value as the 2D CDW.^{19–21} Moreover, the periodicity along c -axis is close to unity, meaning that the 3D CDW modulation is in-phase in neighbouring bilayers.^{19–21} Compared to the 2D short-range CDW, the in-plane and c -axis correlation

lengths are greatly enhanced and extend to the order of 60 lattice constants limited by the instrumental resolution^{19–21} (we call it long-range order). The high field X-Ray measurements have been performed in the doping range $0.10 \leq p \leq 0.12$, where two different Cu–O chain superstructures are observed: ortho II (O-II) for $0.10 \leq p \leq 0.11$ and ortho VIII (O-VIII) for $p \approx 0.12$. The 3D CDW gives rise to an anomaly in the field dependence of the elastic constants via sound velocity measurements²² and of the magnetization.²³ Those two techniques are so far the only thermodynamic probes that have detected a signature of a phase transition towards this 3D CDW state (note that ref. ²³ had different interpretations than the present paper concerning the nature of the low-temperature phase diagram). It has been established by NMR¹⁷ and X-ray^{19–21} measurements that the two charge orders coexist at low temperatures but are related since they share the same periodicity along the b -axis. The coexistence of two distinct charge orders, with different boundaries in the temperature-doping phase diagram raises a certain number of interesting questions: Do both charge orders share the same critical doping? What is their respective impact on the Fermi surface at low temperature? What is the role of disorder in their occurrence?

Here we report a full doping dependence of high field sound velocity measurements, which probe the 3D charge order at low temperatures. Anomalies are now seen in the temperature dependence of sound velocity measured at high field showing a clear negative jump as expected for a second-order phase transition. From the doping dependence of the threshold field H_{CO} and of the onset temperature T_{CO} of the 3D charge order, we find that the two charge orders occur in the same doping range.

We observe that (i) the onset of 3D CDW barely affects the temperature dependence of the Hall coefficient R_H , and (ii) the

¹Laboratoire National des Champs Magnétiques Intenses (LNCMI-EMFL), (CNRS-INSU-UGA-UPS), Toulouse/Grenoble 31400/38042, France; ²Max-Planck-Institut für Festkörperforschung, Heisenbergstrasse 1, Stuttgart D-70569, Germany; ³Karlsruher Institut für Technologie, Institut für Festkörperforschung, Eggenstein-Leopoldshafen D-76344, Germany and ⁴High Field Magnet Laboratory (HFML-EMFL) and Institute for Molecules and Materials, Radboud University, Toernooiveld 7, Nijmegen 6525 ED, The Netherlands Correspondence: Cyril Proust (cyril.proust@lncmi.cnrs.fr) or David LeBoeuf (david.leboeuf@lncmi.cnrs.fr)

Received: 12 June 2017 Revised: 26 January 2018 Accepted: 1 February 2018

Published online: 06 March 2018

sign change of R_H can occur at temperatures as high as 20 K above the onset of 3D CDW. The sign change of the Hall effect, which is observed in the same doping range of YBCO where 2D charge order is found, has been interpreted as a signature of the presence of an electron pocket due to a Fermi surface reconstruction.^{1,24,25} Our results point towards a minor role of the 3D CDW for this reconstruction. A comparison of the 2D CDW correlation length with the quasiparticle de Broglie wavelength furthermore suggests that the 2D CDW can affect the electronic properties above the transition towards 3D CDW.

RESULTS

The sound velocity is defined as $v_s = \sqrt{\frac{c_{ij}}{\rho}}$ for propagation directions along high symmetry axis, where ρ is the density of the material, $c_{ij} = \frac{1}{V} \frac{\partial^2 F}{\partial \epsilon_i \partial \epsilon_j}$, F the free energy, V the volume and ϵ_i the strain. Changes in the elastic constants c_{ij} are expected whenever a strain dependent phase transition occurs.²⁶ This is the case at the superconducting transition where a negative jump of the elastic constant is seen at T_c (see Supplementary Fig. S1). The amplitude of the jump of the elastic constants and of the heat capacity $\Delta C_p(T_c)$ are proportional through the Ehrenfest relation: $\Delta c_{ij}(T_c) = -\frac{\Delta C_p(T_c)}{T_c} \left(\frac{dT_c}{d\epsilon_i} \right)^2$, where the minus sign explains the downward jump in the elastic constant (see discussion in the Supplementary data). This feature is also seen at the onset temperature T_{CO} of the 3D charge order. Indeed, in Fig. 1 we show the in-field temperature dependence of the sound velocity (background subtracted, see Fig. S2 for raw data and fit) in YBCO at three different doping levels. At these dopings, $H_{c2} < 30$ T (ref. ²⁷) such that the normal state is reached down to low temperatures (here by normal state we mean a field-induced state where thermal conductivity,²⁷ heat capacity,²⁸ and NMR knight shift²⁹ have reached a saturating value above a certain field). This feature is the first evidence of a second-order phase transition-like anomaly in the temperature dependence of a thermodynamic probe at T_{CO} . The size of the anomaly is similar for $p = 0.106$ and $p = 0.110$ but it gets smaller for $p = 0.122$. Figure 2a,b show the field dependence up to 35 T of the sound velocity at different temperatures in YBCO at $p = 0.122$. For magnetic field below the

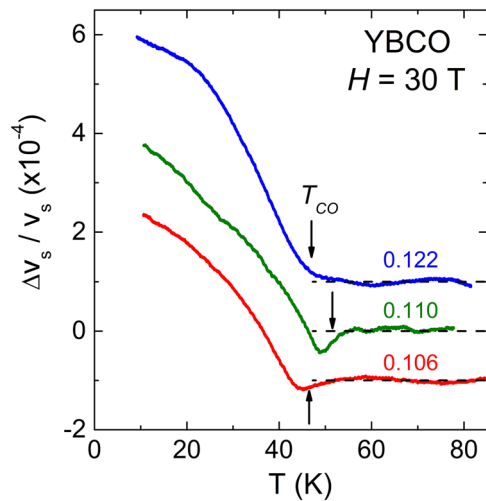


Fig. 1 Sound velocity variation of the longitudinal c_{22} mode (propagation along the b -axis) as a function of temperature measured in YBCO at $p = 0.106$ (red), $p = 0.110$ (green), and $p = 0.122$ (blue) at $H = 30$ T. A lattice background contribution has been subtracted as discussed in the Supplementary. The arrows indicate the charge order transition temperature T_{CO} . Curves are shifted vertically for clarity

irreversibility field, there is a strong contribution from the vortex lattice (see discussion in the Supplementary and Fig. S3). At low fields in the pinned solid vortex phase, the vortex lattice contribution leads to an increase of the sound velocity. This vortex lattice contribution is lost when vortices are depinned leading to a large drop in the sound velocity. The midpoint of this step-like transition associated with vortex depinning is labeled H_v . At field above H_v , the weakening of superconductivity with increasing magnetic field induces a progressive decrease of the sound velocity, until a pronounced hardening of the elastic constant that we attribute to the 3D charge order.²² It leads to a minimum at a field that we define as the threshold charge order field, $H_{CO}(T)$. By performing field sweeps at different temperatures, we can track $H_{CO}(T)$ vs. T and draw up the phase diagram shown in Fig. 2c. Black squares and red circles correspond to $H_v(T)$ and $H_{CO}(T)$, respectively. The phase diagram can be interpreted as follows: at high fields, when superconductivity is mostly suppressed, the charge order transition is field independent, leading to a vertical phase boundary, within our error bars. Due to competition effect when lowering the field close to H_{c2} , superconductivity impedes charge order to appear, pushing the phase

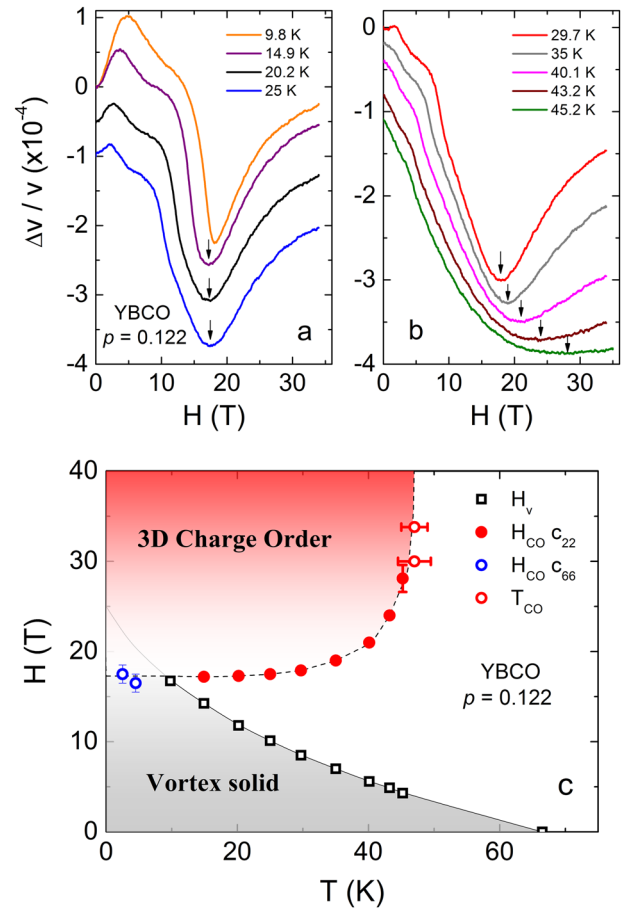


Fig. 2 **a, b** Field dependence of the sound velocity of the c_{22} mode in YBCO ($p = 0.122$) measured at temperatures ranging from 9.8 to 45.2 K. The arrows indicate H_{CO} , the charge order onset field. Curves are shifted vertically for clarity. **c** Temperature–magnetic field phase diagram of YBCO ($p = 0.122$) deduced from sound velocity measurements. H_{CO} (full red circles) and H_v (open black squares) are obtained from measurements shown in the upper panels. T_{CO} (open red circles) is deduced from the temperature dependence of the sound velocity shown in Fig. 1 and Fig. S2. Blue circles correspond to H_{CO} measured at low temperatures using the field dependence of the transverse mode c_{66} (see Fig. S5). Dashed line is a guide to the eye

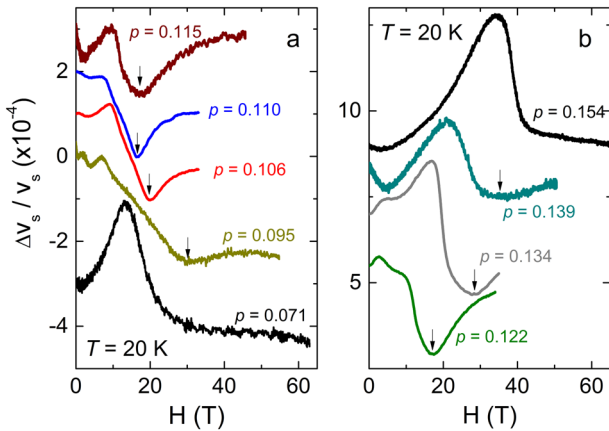


Fig. 3 Field dependence of the sound velocity variation of the c_{22} mode in YBCO at different doping from $p=0.071$ to $p=0.154$ measured at $T=20$ K. Data for $p=0.154$ are divided by a factor 5. Measurements were done either in DC fields up to 37.5 T or in pulsed fields. At $p=0.071$ and $p=0.154$, where no charge order transition is observed, the sound velocity first increases with magnetic field due to the vortex contribution. The large drop signals the loss of this vortex contribution. At still higher fields the sound velocity decreases further as superconductivity is being suppressed by the magnetic field. Those features are also seen at other doping, but a change of slope is observed due to the occurrence of charge order (arrows). Curves are shifted vertically for clarity

boundary, to go almost horizontal such that 3D charge order only appears at finite magnetic field at low T . Similar phase diagram has been obtained by high field X-ray²⁰ and Seebeck coefficient³⁰ measurements. Based on this phase diagram, we define two quantities: $H_{\text{CO}} = H_{\text{CO}}(T \rightarrow 0)$ and T_{CO} which corresponds to the vertical line in Fig. 2c where 3D charge order sets in for $H > H_{\text{c2}}$. Several measurements have been performed in the doping range between $p=0.071$ and $p=0.154$ and Fig. 3 shows the field dependence of the sound velocity at $T=20$ K at all doping. We use the minimum in $\Delta v_s/v_s(H)$ above H_v as a criterion to pinpoint the 3D charge order H_{CO} and extract its doping dependence in the range $p=0.095$ to $p=0.139$ (see Fig. 4a). It is worth noting that the field dependence of the sound velocity above H_v at $p=0.071$ (see curves at different temperatures in Fig. S3b) and $p=0.154$ is featureless. In Fig. S5c, we show the field dependence for $p=0.154$ of the c_{66} mode at $T=4.2$ K, for which there is no sign of transition up to 66 T. We conclude that there is no 3D CDW at these doping levels. The full set of data at all doping along with the temperature–magnetic field phase diagrams deduced from the measurements are shown in the Supplementary Fig. S4 and Fig. S5. The overall shape of these phase diagrams are in agreement with models based on competition between CDW and superconductivity, as discussed below.

DISCUSSION

Indeed, a theory based on a phenomenological nonlinear sigma model which formulates the competition between CDW and fluctuating superconductivity³¹ gives qualitative agreement with the experiment if the effect of disorder is taken into account.^{32,33} Within the model of ref. ³¹ where the effect of magnetic field is incorporated, the onset field for charge order would correspond to a crossover between a short-range 2D CDW order to a long-range 3D CDW at high fields. However, the transition detected by the sound velocity is not a crossover. The presence of a negative jump at T_{CO} (see Fig. 1) clearly indicates the occurrence of a phase transition towards long-range order. Even if theory precludes long-range incommensurate CDW order in disordered systems,

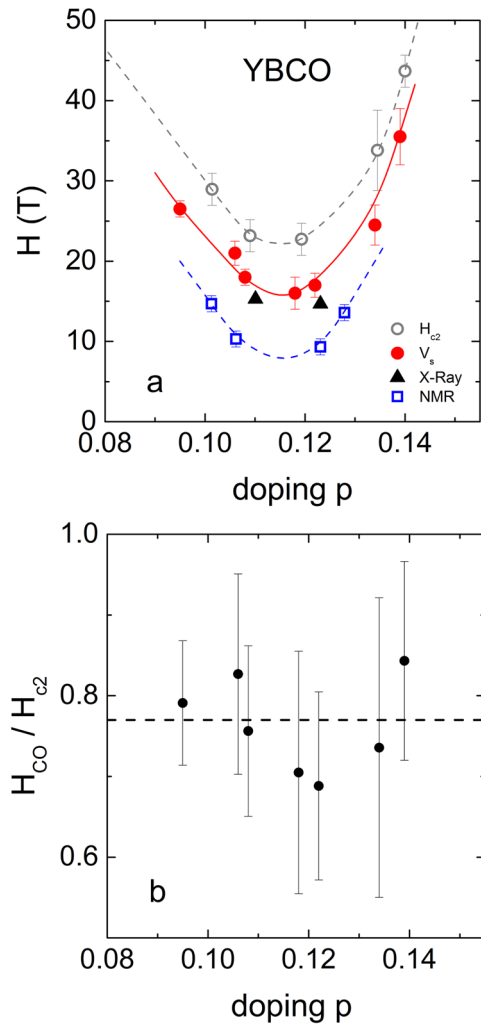


Fig. 4 **a** Magnetic field–doping phase diagram of YBCO comparing H_{CO} and the upper critical field H_{c2} at $T \rightarrow 0$ determined from thermal conductivity and magneto-resistance measurements.²⁷ H_{CO} is determined by NMR^{2,18} (blue squares), X-ray²⁰ (black triangles), and sound velocity (red full circles). Note the good agreement between X-ray and sound velocity data. Sound velocity data at $p=0.108$ was obtained in ref. ²² **b** Doping dependence of the ratio $H_{\text{CO}}/H_{\text{c2}}$, which appears to be almost constant over the entire doping range covered in this study

the notion of “failed thermodynamic transition” has been used to describe the anomaly observed at the temperature/magnetic field where the mean field theory predicts thermodynamic transition. Nevertheless, as the disorder increases, one expects the transition to become more gradual and it leads to crossover. In YBCO, the main source of disorder impacting the CuO_2 planes comes from the CuO chains. This effect is not straightforward to describe in detail but let assume for simplicity that oxygen disorder in the chain layer can create point-like defects (the ends of finite length chainlets) as well as domain walls caused by phase slips in the chain ordering pattern.³⁴ Since the correlation length of the chain order is higher at O-II doping compared to O-VIII and O-III doping,³⁵ it could explain the pronounced anomaly in the temperature dependence of the sound velocity at T_{CO} around O-II doping (see Fig. 1). Another effect that needs certainly to be taken into account is the change in the c -axis correlation length of the CuO chain superstructure order which is finite at O-II doping while the other CuO chain superstructures are mainly 2D. It is

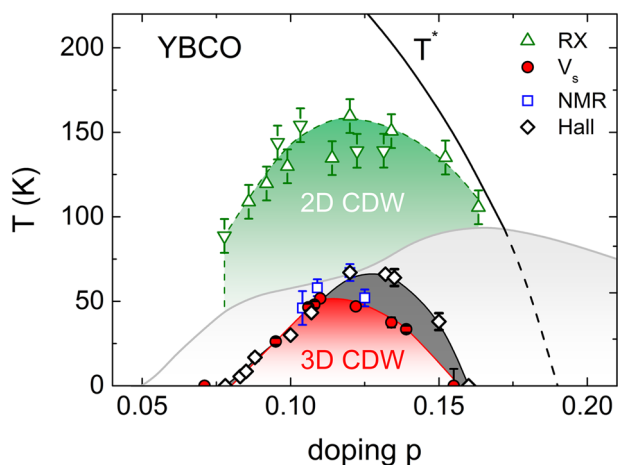


Fig. 5 Phase diagram of charge order in YBCO. Temperature-doping phase diagram of charge orders in YBCO. X-Ray diffraction¹⁶ (down green triangles) and Resonant X-Ray scattering¹⁵ (up green triangles) give the onset temperature of 2D charge order in zero field. The onset temperature of 3D charge order in high fields is given by NMR^{2,18} (blue squares) and sound velocity (red circles). Sound velocity data at $p=0.108$ were obtained in ref.²² A comparison is made with T_0 (black diamonds) the temperature of the sign change of the Hall effect, a signature of an electron pocket in the reconstructed Fermi surface.^{24,25} For $p > 0.11$, the Fermi surface reconstruction takes place at higher temperature than the onset of 3D CDW. Solid black line is the pseudogap temperature T^* in YBCO determined from the resistivity curvature map⁵⁰ Dashed black line is a guide to the eye that extrapolates to the critical point of the pseudogap $p^* = 0.19$ (ref.³⁸), that is distinct from the critical point of the CDW

conceivable that disorder in the chain structure along the c -axis for oxygen content away from O-II could smear out the transition towards the 3D CDW. While the nonlinear sigma model succeeds to explain most of the salient feature related to the 2D/3D CDW, one must admit that the situation is more complex in YBCO since it has been found that the 3D ordered CDW at high fields develops on top of the 2D CDW and it is not simply a crossover, that is to say they coexist at low temperature in the presence of a magnetic field.³⁶ In addition, the two charge orders differ in the sense that the 3D CDW is 3D ordered but with uniaxial modulation along the b -axis in the plane (although with the same wave vector than the 2D CDW).

To reconcile the two closely related but yet distinct charge orders coexisting at low temperature, it has been proposed in ref.²¹ that the coexistence is inhomogeneous depending on the non-uniform distribution of the disorder strengths in the sample. Another scenario comes from a recent extension of the nonlinear sigma model of competing superconducting and CDW orders. This model shows that the coexistence of the two CDWs could be a consequence of the interplay between the disorder potential (that prevails at zero magnetic field) and the Coulomb interaction between CDWs on different CuO_2 planes, that plays a more important role when magnetic field is applied.³⁶

In our previous paper,²² the sound velocity anomalies found at H_{CO} had been interpreted as being caused by a bi-axial order, as suggested by X-ray measurements.^{3,4} This interpretation was based on a group theory analysis of different acoustic modes. The fact that anomalies have been detected in all measured acoustic modes is not straightforward to reconcile with only a uniaxial CDW. The recent discovery of the field-induced long-range order with uniaxial character that coexists with the 2D CDW increases the level of complexity in terms of coupling of the order parameters. It is natural to interpret the sound velocity anomalies as being due to the uniaxial order since it corresponds to long-

range order. A more thorough analysis, including the coupling between both charge modulations and superconductivity, the coupling to the lattice, and the effect of magnetic field, remains to be done in order to understand the impact of the charge modulations on the magnetic field dependence of the sound velocity.

From the temperature sweeps shown in Fig. 1 and the phase diagrams at different doping levels, we were able to compile the doping dependence of the onset field H_{CO} and the onset temperature T_{CO} of the 3D CDW shown in Figs. 4 and 5, respectively. In Fig. 4a, the doping dependence of H_{CO} shows that it is systematically lower than $H_{\text{c}2}$. Figure 4b shows that in the limit $T \rightarrow 0$, 3D charge order always appears around $H_{\text{CO}} \approx 0.8 H_{\text{c}2}$, despite the pronounced doping dependence of the ratio T_{CO}/T_c (Note that a fixed relation between H_{CO} and $H_{\text{c}2}$, in a limited doping range, has been discussed in refs.^{18,21}). Figure 4a reveals also that NMR gives lower H_{CO} than sound velocity measurements. The observation of in-plane precursor correlations of the 3D charge order²⁰ can explain this difference. NMR would be sensitive to this precursor phase but not sound velocity since it is a thermodynamic probe and hence is mostly sensitive to the onset of a 3D long-range, static order parameter. H_{CO} measured by sound velocity is in better agreement with thermal Hall effect,³⁷ X-ray,^{19–21} and recent Seebeck coefficient³⁰ measurements in finite magnetic field. In Fig. 5 we plot the onset temperatures T_{CO} for the 3D ordered CDW. The comparison of T_{CO} with the 2D CDW onset temperatures deduced from X-ray measurements^{15,16} leads to our first main finding: 2D and 3D CDW occur in the same doping range, within experimental accuracy. In other words, the charge orders are intimately linked even though the situation does not correspond to a crossover between the two. Note that the putative critical point of pseudogap ($p^* \sim 0.19$ from ref.³⁸) and of CDW are distinct and well separated, in agreement with Hall effect measurements.³⁹ But it raises the question: why both charge orders occur only in such limited doping range? In YBCO spin density wave (SDW) occurs for $p < 0.08$ and the competition between SDW and CDW⁴⁰ can explain the location of the critical point at $p \approx 0.08$. On the right side of the CDW dome ($p \approx 0.16$), assuming that the proximity of the critical point of the pseudogap ($p = 0.19$) leads to a change in the carrier density,³⁹ thus in the Fermi surface topology, it can be detrimental for charge order.

Let us discuss our finding in the context of Fermi surface reconstruction. It has been suggested that the negative Hall coefficient is a signature of an electron pocket resulting from a reconstruction of the Fermi surface by the charge order.^{24,25} This interpretation relies on the concept of Fermi liquid and Landau quasiparticles, which is strictly valid at low temperature where quantum oscillations are observed, e.g. $T < 20$ K (ref.⁴¹). At higher temperature, the quasiparticles are ill-defined in particular near the Brillouin zone boundaries (the anti-nodal direction)⁴² and the concept of Fermi surface reconstruction might not apply. However, through our discussion, we will assume that the concept of quasiparticle is valid at high temperature (e.g. quasiparticles near the nodal direction of the Fermi surface) and use simple arguments that describe conventional CDW systems although the situation is more complex in YBCO.

Our direct determination of the 3D CDW onset allows studying its impact on transport properties such as the Hall effect reported in the literature.^{24,25} In Fig. 5 we compare the onset temperature T_{CO} of the 3D CDW deduced from ultrasound and NMR measurements¹⁸ with T_0 , the temperature where the Hall coefficient R_H changes sign.^{24,25} While $T_0 \approx T_{\text{CO}}$ for $p \leq 0.11$, R_H becomes negative at temperature higher than the onset temperature of 3D CDW for $p > 0.11$. To better illustrate this fact we compare in Fig. 6a the in-field temperature dependence of the sound velocity and of the Hall effect for $p = 0.12$, which shows that 3D CDW appears 20 K below the sign change in the Hall

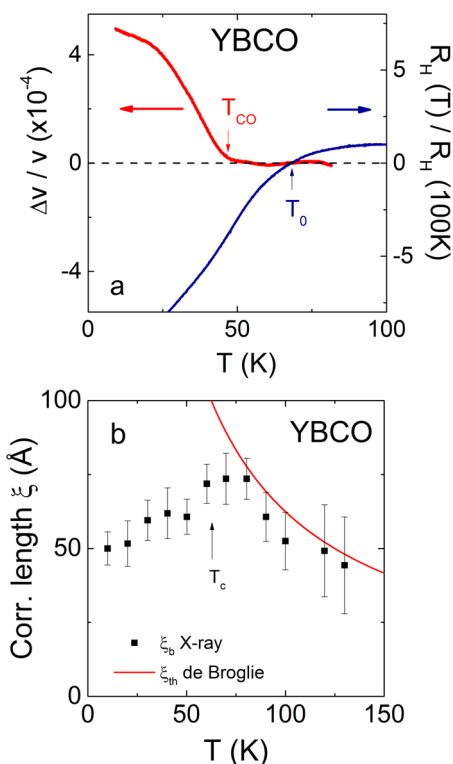


Fig. 6 **a** Comparison of the temperature dependence of the sound velocity induced by 3D charge order in YBCO at $p = 0.122$ and at $H = 30$ T (red curve) and of the Hall coefficient in a YBCO sample at similar doping ($p = 0.12$) and $H = 45$ T (blue curve, from ref. ²⁴). At this doping, the Hall coefficient has negligible field dependence between $H = 30$ and $H = 45$ T making this comparison relevant (see Fig. S1b of ref. ²⁴). Note that R_H changes sign 20 K above the onset of 3D charge order. **b** Temperature dependence of the correlation length of the 2D charge order¹⁵ in YBCO O-II (black squares) and of the de Broglie wavelength (red line, see text)

coefficient. In addition, the onset of 3D CDW has little impact on the behavior of R_H .

This begs the question of how the low-lying (near-nodal) electronic states evolves through the charge ordering transitions in YBCO and which electronic order causes the Fermi surface reconstruction observed at low temperatures. The simplest explanation would be that the Fermi surface reconstruction process is governed by 2D CDW for $p > 0.11$, unambiguously observed by NMR and X-Ray. While we cannot exclude that another unidentified electronic order is responsible for the Fermi surface reconstruction, let us examine whether 2D CDW short-range correlations are enough to impact the electronic structure for temperatures above T_{CO} . In 2D systems, it has been theoretically demonstrated that antiferromagnetic fluctuations with correlation length becoming much greater (as T is lowered) than the quasiparticle de Broglie wavelength $\xi_{th} = \hbar v_F / k_B T$ can cause changes in the low-lying electronic states.⁴³ Here we apply this concept to the 2D charge order in YBCO, that is, the thermal de Broglie wavelength ξ_{th} should be compared with the correlation length of the 2D charge order ξ_{CO} . If $\xi_{CO} \gg \xi_{th}$ quasiparticles become sensitive to the charge order correlations, which might lead to a Fermi surface reconstruction. Although this estimation is approximate, we use the average Fermi velocity v_F deduced from quantum oscillations,⁴⁴ $F = 540$ T and $m^* = 1.8m_e$ leading to $v_F = 8.2 \cdot 10^4 \text{ m s}^{-1}$. In Fig. 6b, we compare the temperature dependence of ξ_{th} and of the 2D charge order correlation length¹⁵ measured in O-II YBCO in zero field. The de

Broglie wavelength follows closely the correlation length of the charge order above T_c and up to the temperature where the 2D charge order appears. Though the result of ref. ⁴³ is strictly valid if $\xi_{CO} \gg \xi_{th}$, our comparison of the thermal wavelength and 2D CDW correlation length suggest that 2D short-range CDW correlation can impact low-lying (near-nodal) electronic states at high temperatures. An extension of the calculation of ref. ⁴³ for charge order would be helpful to the present discussion.

At low temperatures, our interpretation leads to another question: Is the 2D CDW correlation length compatible with the quasiparticle mean free path inferred from quantum oscillations? In Fig. S6 we compare the quasiparticle mean free path deduced from quantum oscillation experiments with $\xi_{CO}(T = T_c)$, at different doping levels in YBCO. We see that, except for well-ordered YBCO O-II ($p \sim 0.11$), the two length scales are comparable, suggesting that quasiparticle mean free path is bounded by the 2D charge order correlation length. This observation further supports the scenario that the Fermi surface reconstruction is governed by the 2D CDW. Note that the two length scales might be limited due to a significantly enhanced quasiparticle scattering originating in the shorter correlation lengths of their CuO chain ordering.^{35,45} However, for YBCO O-II the mean free path is much longer than the 2D charge order correlation length and is comparable to the 3D charge order correlation length. Given that the wave vector of the modulation is close to a commensurate number ($\delta_b \approx 0.33$ from ref. ²¹), it is tempting to invoke a ‘lock-in’ transition at high fields at this particular oxygen ordering, leading to a strong enhancement of the correlation length of both charge order. Note that if the Fermi surface is already reconstructed by the 2D charge order at high temperature, the occurrence of the 3D charge order with the same wave vector along the b -axis would not strongly affect the reconstructed Fermi surface.

This overall scenario would explain the negative Hall and Seebeck coefficients in $\text{HgBa}_2\text{CuO}_4$ (ref. ⁴⁶) and $\text{La}_{2-x}\text{Sr}_x\text{CuO}_4$ (ref. ⁴⁷) where only short-range charge orders have been observed^{5,48,49} and long-range charge order has been missing so far.

METHODS

Samples and experimental technique

The samples are detwinned single crystals of $\text{YBa}_2\text{Cu}_3\text{O}_y$ grown by the self-flux method.

The oxygen atoms in the CuO chains were made to order into the stable superstructure specific to the given oxygen concentration y . Samples with oxygen content $y = 6.55$ and $y = 6.51$ with ortho II order showed nice quantum oscillations in the sound velocity and attenuation (not shown), indicating high sample quality. The superconducting critical temperature T_c were determined using the measurement of the elastic constant c_{22} and are reported in Table S1. The hole carrier concentration is deduced from the measurement of T_c and the c -axis lattice parameter, using a relationship between T_c , c -axis lattice parameter and doping in the CuO_2 planes.

Longitudinal (transverse) ultrasonic waves were generated using commercial LiNbO_3 36° Y-cut (41° X-cut) transducers glued on oriented, polished, cleaned surfaces. The standard pulse-echo technique with phase comparison was used to measure sound velocity variation.

Experiments have been conducted in static field at the HFML, Nijmegen and the LNCMI, Grenoble, and in pulsed field at the LNCMI-Toulouse. The magnetic field was applied along the c -axis of the orthorhombic structure of YBCO.

Data availability

All relevant data are available upon request from the corresponding authors.

ACKNOWLEDGEMENTS

This work was performed at the HFML and the LNCMI, members of the European Magnetic Field Laboratory (EMFL). C.P. acknowledges funding from the French ANR (SUPERFIELD, contract ANR-12-BS04-0012-02) the Laboratoire d'Excellence NEXT (ANR-10-LABX-0037-NEXT). D.L. acknowledges funding from the French ANR (project UNESCOS, contract ANR-14-CE05-0007), the Laboratoire d'Excellence LANEF (ANR-10-LABX-51-01) and the Université Grenoble-Alpes (SMLng-AGIR). The authors wish to thank J. Chang, M. Dion, M.-H. Julien, T. Klein, C. Marcenat, H. Mayaffre, D. Orgad, I. Paul, R. Ramazashvili, Y. Sidis, W. Tabis, L. Taillefer, B. Vignolle, D. Vignolles, I. Vinograd and more particularly S. Kivelson and A.-M. Tremblay, for stimulating and fruitful discussions.

AUTHOR CONTRIBUTIONS

J.P., T.L., M.L.T., and B.K. grew, prepared (annealing, de-twinning), and characterized the samples. F.L., S.B., M.F., B.B., C.P., and D.L. performed the high magnetic field measurements. S.W. provided instrumental support for the DC field experiment at HMFL. F.L., S.B., M.F., and D.L. carried out the data analysis. C.P. and D.L. wrote the manuscript with inputs from all co-authors.

ADDITIONAL INFORMATION

Supplementary information accompanies the paper on the *npj Quantum Materials* website (<https://doi.org/10.1038/s41535-018-0084-5>).

Competing interests: The authors declare no competing interests.

Publisher's note: Springer Nature remains neutral with regard to jurisdictional claims in published maps and institutional affiliations.

REFERENCES

- Sebastian, S. E. & Proust, C. Quantum oscillations in hole-doped cuprates. *Annu. Rev. Condens. Matter Phys.* **6**, 411–430 (2015).
- Wu, T. et al. Magnetic-field-induced charge-stripe order in the high-temperature superconductor $\text{YBa}_2\text{Cu}_3\text{O}_y$. *Nature* **477**, 191–194 (2011).
- Ghiringhelli, G. et al. Long-range incommensurate charge fluctuations in $(\text{Y,Nd})\text{Ba}_2\text{Cu}_3\text{O}_{6+x}$. *Science* **337**, 821–825 (2012).
- Chang, J. et al. Direct observation of competition between superconductivity and charge density wave order in $\text{YBa}_2\text{Cu}_3\text{O}_{6.67}$. *Nat. Phys.* **8**, 871–876 (2012).
- Tabis, W. et al. Charge order and its connection with Fermi-liquid charge transport in a pristine high- T_c cuprate. *Nat. Commun.* **5**, 5875 (2014).
- Fradkin, E., Kivelson, S. A. & Tranquada, J. M. Theory of intertwined orders in high temperature superconductors. *Rev. Mod. Phys.* **87**, 457–482 (2015).
- Vojta, M. Lattice symmetry breaking in cuprate superconductors: stripes, nematics, and superconductivity. *Adv. Phys.* **58**, 699–820 (2009).
- Efeto, K. B., Meier, H. & Pépin, C. Pseudogap state near a quantum critical point. *Nat. Phys.* **9**, 442–446 (2013).
- Sachdev, S. & La Placa, R. Bond order in two-dimensional metals with anti-ferromagnetic exchange interactions. *Phys. Rev. Lett.* **111**, 027202 (2013).
- Wang, Y. & Chubukov, A. V. Charge-density-wave order with momentum $(2Q,0)$ and $(0,2Q)$ within the spin-fermion model: continuous and discrete symmetry breaking, preemptive composite order, and relation to pseudogap in hole-doped cuprates. *Phys. Rev. B* **90**, 035149 (2014).
- Lee, P. A. Amperean pairing and the pseudogap phase of cuprate superconductors. *Phys. Rev. X* **4**, 031017 (2014).
- Caprara, S., Di Castro, C., Seibold, G. & Grilli, M. Dynamical charge density waves rule the phase diagram of cuprates. *Phys. Rev. B* **95**, 224511 (2017).
- Montiel, X., Kloss, T. & Pépin, C. Effective $\text{SU}(2)$ theory for the pseudogap state. *Phys. Rev. B* **95**, 104510 (2017).
- Liu, Y.-H. et al. Giant phonon anomaly associated with superconducting fluctuations in the pseudogap phase of cuprates. *Nat. Commun.* **7**, 10378 (2016).
- Blanco-Canosa, S. et al. Resonant x-ray scattering study of charge-density wave correlations in $\text{YBa}_2\text{Cu}_3\text{O}_{6+x}$. *Phys. Rev. B* **90**, 054513 (2014).
- Hücker, M. et al. Competing charge, spin, and superconducting orders in underdoped $\text{YBa}_2\text{Cu}_3\text{O}_y$. *Phys. Rev. B* **90**, 054514 (2014).
- Wu, T. et al. Incipient charge order observed by NMR in the normal state of $\text{YBa}_2\text{Cu}_3\text{O}_y$. *Nat. Commun.* **6**, 6438 (2015).
- Wu, T. et al. Emergence of charge order from the vortex state of a high-temperature superconductor. *Nat. Commun.* **4**, 2113 (2014).
- Gerber, S. et al. Three-dimensional charge density wave order in $\text{YBa}_2\text{Cu}_3\text{O}_{6.67}$ at high magnetic fields. *Science* **350**, 949–952 (2015).
- Chang, J. et al. Magnetic field controlled charge density wave coupling in underdoped $\text{YBa}_2\text{Cu}_3\text{O}_{6+x}$. *Nat. Commun.* **7**, 11494 (2016).
- Jang, H. et al. Ideal charge-density-wave order in the high-field state of superconducting YBCO. *Proc. Natl. Acad. Sci. USA* **113**, 14645–14650 (2016).
- LeBoeuf, D. et al. Thermodynamic phase diagram of static charge order in underdoped $\text{YBa}_2\text{Cu}_3\text{O}_y$. *Nat. Phys.* **9**, 79–83 (2013).
- Yu, F. et al. Magnetic phase diagram of underdoped $\text{YBa}_2\text{Cu}_3\text{O}_y$ inferred from torque magnetization and thermal conductivity. *Proc. Natl. Acad. Sci. USA* **113**, 12667–12672 (2016).
- LeBoeuf, D. et al. Electron pockets in the Fermi surface of hole-doped high- T_c superconductors. *Nature* **450**, 533–536 (2007).
- LeBoeuf, D. et al. Lifshitz critical point in the cuprate superconductor $\text{YBa}_2\text{Cu}_3\text{O}_y$ from high-field Hall effect measurements. *Phys. Rev. B* **83**, 054506 (2011).
- Lüthi, B. *Physical Acoustics in the Solid State*, Springer Series for Solid-State Sciences, Vol. 148 (Springer, Berlin, New York, 2005).
- Grissonnanche, G. et al. Direct measurement of the upper critical field in cuprate superconductors. *Nat. Commun.* **5**, 3280 (2014).
- Marcenat, C. et al. Calorimetric determination of the magnetic phase diagram of underdoped Ortho-II YBCO single crystals. *Nat. Commun.* **6**, 7927 (2015).
- Zhou, R. et al. Spin susceptibility of charge ordered $\text{YBa}_2\text{Cu}_3\text{O}_y$ across the upper critical field. *Proc. Natl. Acad. Sci. USA* **114**, 13148–13153 (2017).
- Cyr-Choinière, O. et al. Anisotropy of the seebeck coefficient in the cuprate superconductor $\text{YBa}_2\text{Cu}_3\text{O}_y$: Fermi-surface reconstruction by bidirectional charge order. *Phys. Rev. X* **7**, 031042 (2017).
- Hayward, L. E. et al. Angular fluctuations of a multicomponent order describe the pseudogap of $\text{YBa}_2\text{Cu}_3\text{O}_{6+x}$. *Science* **343**, 1336–1339 (2014).
- Nie, L. et al. Fluctuating orders and quenched randomness in the cuprates. *Phys. Rev. B* **92**, 174505 (2015).
- Caplan, Y., Wachtel, G. & Orgad, D. Long-range order and pinning of charge-density waves in competition with superconductivity. *Phys. Rev. B* **92**, 224504 (2015).
- Achkar, A. J. et al. Impact of quenched oxygen disorder on charge density wave order in $\text{YBa}_2\text{Cu}_3\text{O}_{6+x}$. *Phys. Rev. Lett.* **113**, 107002 (2014).
- Zimmermann, M. V. et al. Oxygen-ordering superstructures in underdoped $\text{YBa}_2\text{Cu}_3\text{O}_{6+x}$ studied by hard x-ray diffraction. *Phys. Rev. B* **68**, 104515 (2003).
- Caplan, Y. & Orgad, D. Dimensional crossover of charge-density wave correlations in the cuprates. *Phys. Rev. Lett.* **119**, 107002 (2017).
- Grissonnanche, G. et al. Onset field for Fermi-surface reconstruction in the cuprate superconductor $\text{YBa}_2\text{Cu}_3\text{O}_y$. Preprint at <http://arXiv.org/abs/1508.05486> (2015).
- Tallon, J. L. & Loram, J. W. The doping dependence of T^* —what is the real high- T_c phase diagram? *Phys. C* **349**, 53–68 (2001).
- Badoux, S. et al. Change of carrier density at the pseudogap critical point of a cuprate superconductor. *Nature* **531**, 210–214 (2016).
- Blanco-Canosa, S. et al. Momentum-dependent charge correlations in $\text{YBa}_2\text{Cu}_3\text{O}_{6+\delta}$ superconductors probed by resonant X-ray scattering: evidence for three competing phases. *Phys. Rev. Lett.* **110**, 187001 (2013).
- Senthil, T. & Lee, P. A. Synthesis of the phenomenology of the underdoped cuprates. *Phys. Rev. B* **79**, 245116 (2009).
- Damascelli, A., Hussain, Z. & Shen, Z. X. Angle-resolved photoemission studies of the cuprate superconductors. *Rev. Mod. Phys.* **75**, 473 (2003).
- Vilk, Y. & Tremblay, A.-M. Non-perturbative many-body approach to the Hubbard model and single-particle pseudogap. *J. Phys. I France* **7**, 1309 (1997).
- Doiron-Leyraud, N. et al. Quantum oscillations and the Fermi surface in an underdoped high- T_c superconductor. *Nature* **447**, 565–568 (2007).
- Bobowski, J. S. et al. Oxygen chain disorder as the weak scattering source in $\text{YBa}_2\text{Cu}_3\text{O}_{6.50}$. *Phys. Rev. B* **82**, 134526 (2010).
- Doiron-Leyraud, N. et al. Hall, Seebeck, and Nernst coefficients of underdoped $\text{HgBa}_2\text{CuO}_{4+\delta}$: Fermi-surface reconstruction in an archetypal cuprate Superconductor. *Phys. Rev. X* **3**, 021019 (2013).
- Badoux, S. et al. Critical doping for the onset of Fermi-surface reconstruction by charge-density-wave order in the cuprate superconductor $\text{La}_{2-x}\text{Sr}_x\text{CuO}_4$. *Phys. Rev. X* **6**, 021004 (2016).
- Croft, T. P., Lester, C., Senn, M. S., Bombardi, A. & Hayden, S. M. Charge density wave fluctuations in $\text{La}_{2-x}\text{Sr}_x\text{CuO}_4$ and their competition with superconductivity. *Phys. Rev. B* **89**, 224513 (2014).
- Thampy, V. et al. Rotated stripe order and its competition with superconductivity in $\text{La}_{1.88}\text{Sr}_{0.12}\text{CuO}_4$. *Phys. Rev. B* **90**, 100510(R) (2014).
- Ando, Y. et al. Electronic phase diagram of high- T_c cuprate superconductors from a mapping of the in-plane resistivity curvature. *Phys. Rev. Lett.* **93**, 267001 (2004).



Open Access This article is licensed under a Creative Commons Attribution 4.0 International License, which permits use, sharing, adaptation, distribution and reproduction in any medium or format, as long as you give appropriate credit to the original author(s) and the source, provide a link to the Creative Commons license, and indicate if changes were made. The images or other third party material in this article are included in the article's Creative Commons license, unless indicated otherwise in a credit line to the material. If material is not included in the

article's Creative Commons license and your intended use is not permitted by statutory regulation or exceeds the permitted use, you will need to obtain permission directly from the copyright holder. To view a copy of this license, visit <http://creativecommons.org/licenses/by/4.0/>.

© The Author(s) 2018